

LD-SDM: Language-Driven Hierarchical Species Distribution Modeling

Srikumar Sastry¹, Xin Xing², Aayush Dhakal¹, Subash Khanal¹, Adeel Ahmad^{1,3}, Nathan Jacobs¹
¹Washington University in St. Louis, ²University of Kentucky, ³Taylor Geospatial Institute

Abstract

We focus on the problem of species distribution modeling using global-scale presence-only data. Most previous studies have mapped the range of a given species using geographical and environmental features alone. To capture a stronger implicit relationship between species, we encode the taxonomic hierarchy of species using a large language model. This enables range mapping for any taxonomic rank and unseen species without additional supervision. Further, we propose a novel proximity-aware evaluation metric that enables evaluating species distribution models using any pixel-level representation of ground-truth species range map. The proposed metric penalizes the predictions of a model based on its proximity to the ground truth. We describe the effectiveness of our model by systematically evaluating on the task of species range prediction, zero-shot prediction and geo-feature regression against the state-of-the-art. Results show our model outperforms the strong baselines when trained with a variety of multi-label learning losses.

1. Introduction

The ever-increasing availability of crowdsourced and remote sensing data has opened opportunities to solving challenging tasks that were not possible before. One such task is global-scale joint species distribution modeling (SDM). Understanding species ranges is not only essential for biodiversity conservation but also for understanding the effects of climate change. However, complex biophysical and geographic processes make SDM a challenging task.

Traditionally, species ranges were mapped using geographical and environmental features. While the current approaches have their merits, we contend they fall short in accurately representing the inter-species relationships inherent in the taxonomic hierarchy. For example, *species* belonging to the same *genera* tend to be found in similar locations. They often share many common characteristics, including their general habitat preferences [41]. Nevertheless, this pattern diminishes as one moves up in the taxonomic hierarchy. To capture these complex hierarchical relationships

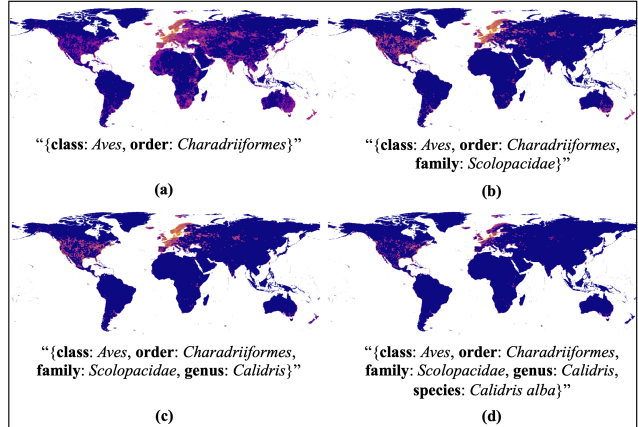


Figure 1. **Species Distribution Modeling using LLM Guidance.** We use text prompts in the form of key-value pairs for training our species distribution model. This kind of prompt captures the taxonomy hierarchy of species. We use only the exhaustive prompt (d) for training while the rest are used for zero-shot predictions.

between the species, we use large language models (LLMs) to encode their taxonomic information in text (as shown in Figure 1). Intuitively, this should enhance the identification of rare taxa [9]. To the best of our knowledge, no previous work has incorporated large language models for SDM.

In order to incorporate species-specific embeddings into SDM, it is necessary to reformulate the SDM problem. Previous approaches to SDM [15, 24, 27] tried to answer the question, “which species are likely to be found at a given location?”. In contrast, our approach to SDM models, “which locations are likely for a given species to be found?”. Assuming uniform prior over the species distribution [24, 27], this is an equivalent formulation as before. But by doing so, we can now incorporate a variety of information, including species-specific embeddings or any other metadata, which opens up new opportunities for more accurate modeling. Alternatively, this formulation makes it easier to incorporate unseen species that were not present in the training data.

Previously, SDMs were trained using environmental features while ignoring the geographic location aspect. Recently, several works showed the benefit of incorporat-

ing geographic locations in various applications including SDM [6, 15, 38] and fine-grained image classification [2, 12, 27]. A series of works [5, 34] proposed spherical harmonics representation of geographic location. Inspired by these works, we propose to use the Spherical Fourier Neural Operators (SFNO’s) [5] as a geographical and environmental feature extractor for SDM.

When it comes to predicting species range, the evaluation process typically involves using range maps that are defined by experts or curated carefully [29, 43]. However, these maps can often be sparse and difficult to obtain. Alternatively, using any crowdsourced species observation data can also be challenging as there is no precise definition of species absence. Intuitively, models with false predictions close to their true locations are better than those with distant false predictions. This is because models in the former case learn *spatially localized* species distributions. Previous studies have used the area under the curve (AUC) [29, 43] and the mean average precision (MAP) [15] to evaluate SDMs. However, these metrics ignore the spatial distribution of predictions and weigh them equally, making them highly sensitive to spatial shifts in the predictions. Even a single pixel-level shift in predictions could add significant bias to the scores.

To this end, we propose a proximity-adjusted evaluation metric that penalizes predictions based on their distance to the closest true locations. We construct a One-Way Probability-Weighted Chamfer Distance (PWCD) metric, that measures the dissimilarity between the true and predicted species range maps, which is robust to small shifts. This enables an effective evaluation of SDMs using pixel-level range maps and crowdsourced data (where absence is not confirmed).

The contribution of our work is threefold:

1. We use large language models to encode taxonomic information of species, which allows mapping over any taxonomic level.
2. We reformulate the SDM problem which enables the use of species-specific embeddings. This allows inference on unseen species.
3. We propose a novel proximity-aware metric for assessing the performance of SDMs using pixel-level range maps.

2. Related Works

Species distribution modeling (SDM) is a set of techniques that uses environmental, geographic, and species observation data to predict species distribution across geographic space and time [4, 16]. In this context, we restrict ourselves to the task of species range mapping over geographic space only. In the past, SDM relied on hand-crafted geographic and environmental features as input to capture the implicit spatial correlations in data [17, 29, 43]. These ap-

proaches were limited to one species per model due to their reliance on traditional supervised learning algorithms. With advancements in deep neural network architectures, end-to-end frameworks are now able to model joint species distributions and complex implicit relations in data [6, 10, 15].

Another important aspect of SDM is the type of species occurrence data. Species occurrence data may exist in one of the two forms: *presence-only* and *presence-absence*. Collecting presence-absence observations is a challenging task, requiring expert surveys especially to confirm the absence of a given species in some region [28]. However, once collected, this kind of data can be easily fed into supervised learning frameworks, without requiring sophisticated modifications [6, 11, 19, 20, 40]. With no expert knowledge, presence-only data can be recorded when any species of interest is encountered. This way of collecting data does not require the data collector to confirm absences. However, since there are no negative samples, it is difficult to use standard supervised learning frameworks [8, 10, 22].

Most of the recent works formulate the problem of SDM using presence-only data as a multi-label classification task [15, 27]. Here, the goal of SDM is to predict the likelihood over species for a given location and environmental features. A variety of multi-label learning losses have been proposed in the literature that can easily be plugged in for this task. For instance, the AN-full (full assume negative) loss [27] randomly samples locations that are assumed to be negative during training. The ME-full (full maximum entropy) [49] tries to maximize the entropy of predictions of negative samples and at randomly sampled locations during training. Other losses such as ASL (asymmetric loss) [32], Hill loss [48], and RAL (robust asymmetric loss) [31] weigh the negative samples in a way that easy negative and potential false negative samples are down-weighted. The authors of [15] presented an extensive comparison of the performance of SDMs trained with losses involving pseudo-negative sampling. Here, we extend their work by additionally comparing their SDMs trained with the ASL and RAL losses.

Several studies have attempted to assess the performance of species distribution models trained on presence-only data [23, 29, 36, 43, 45]. They measure performance using Kappa index, Kullback–Leibler divergence, area under the curve (AUC), or mean average precision (MAP). However, these metrics are inadequate in quantifying the performance of models on pixel-level data. It is worth noting that none of these metrics consider the spatial proximity of predictions to their ground-truth observations, hence making them sensitive to spatial shifts in predictions.

Finally, another line of work uses high-resolution satellite imagery at each species occurrence location to guide SDM methods [7, 13, 25, 26, 35, 39]. For example, [39] uses satellite imagery and geolocation to directly predict

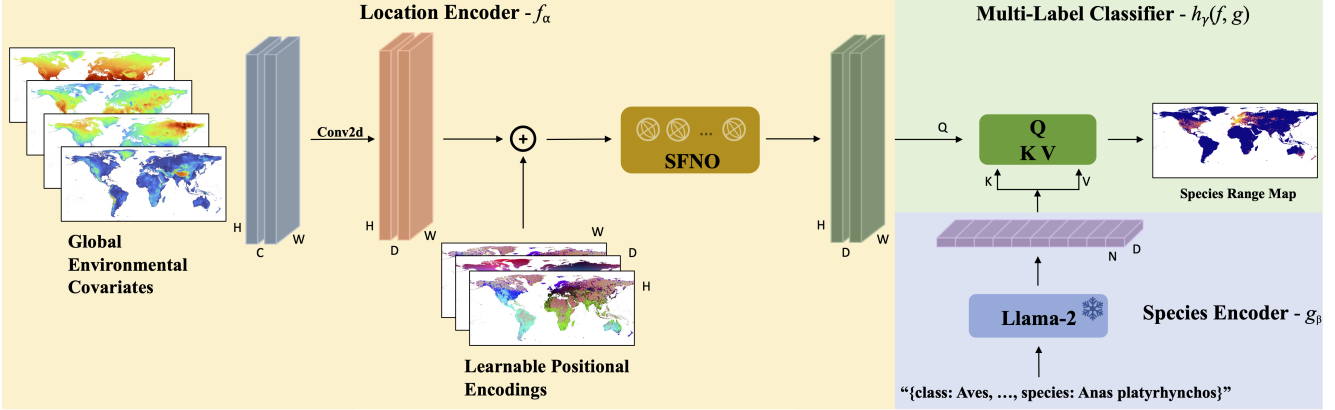


Figure 2. **Proposed Architecture.** During training, features extracted from the environmental covariates are added to a learnable positional embedding and passed to the spherical Fourier neural network (SFNO). The species range map is obtained by computing cross-attention between the representations from SFNO and embeddings obtained from LLaMA-2 for a text description of a given species. Inference requires only cross-attention computation if embeddings are precomputed.

the likelihood over species while [35] uses a contrastive learning framework to establish similarity between ground-level images of species and corresponding satellite imagery. These methods are limited in geographic scale due to the high-resolution nature of raw data [15]. Except [39], all the works view this problem as an information retrieval task rather than a species prediction task.

3. Method

In this section, we describe our approach to hierarchical species distribution modeling with LLMs.

3.1. Problem Definition

We consider presence-only data in the form of occurrence records: $\mathcal{D} = \{(l_i, y_i) \mid i = 1, \dots, N\}$, where $l_i \in \mathbb{R}^2$ is the geolocation of each observation and $y_i \in [1, \dots, S]$ is the species of the observed organism. Additionally, a set of environmental features $e_i \in \mathbb{R}^n$ is included for each location l_i . Many previous studies [15, 24, 27] have tackled the task of SDM by training a neural network to model the conditional probability of $p(y \mid l, e)$. This translates to the problem of “how likely a *species* can be found at a given *location*”. However, our approach involves modeling the probability of $p(r \mid y, l_r, e_r)$, which answers the question “Is it likely for a given species to be found at given location?”. Here, $r \in [1, \dots, L]$ is a set of discrete locations that are of interest when predicting the range of species belonging to some class. In this framework, we define the set of locations r as a contiguous grid that is laid over the surface of the globe. The variables l_r and e_r represent fixed parameters in the model, namely the location vectors and environmental features defined at each location in r respectively. It is easy to see that the input y and the parameters (l_r, e_r)

can have any arbitrary representations. So, this new formulation allows for flexible encoding of both the species class and geographic location, compared to the previous formulation which only allowed flexibility in representing the geographic location.

3.2. Architecture Overview

Our objective is to train a neural network of the form: $f_\theta(y; l_r, e_r) : \mathbb{R}^d \rightarrow [0, 1]^L$, where d is the dimensionality of the species feature vector. f_θ is composed of three modules: 1) a location encoder network f_α , 2) a species encoder network g_β , and 3) a multi-label classifier h_γ . See Figure 2 for a high-level architecture diagram. The network f_α consists of convolutional feature extractors and the Spherical Fourier Neural Operator (SFNO) [5] blocks that take as input the fixed parameters: l_r and e_r . The location vectors are used as learnable positional encodings for the SFNO blocks. The species encoder g_β takes as input the text descriptions corresponding to a particular species of class y . The multi-label classifier h_γ consists of a cross-attention network that fuses features from the SFNO and text encoder and performs multi-label classification using a linear layer. We call our model Language-Driven Species Distribution Model (LD-SDM).

3.3. Species-specific embeddings

Many popular crowdsourcing science platforms, such as iNaturalist [44], contain not just occurrence records, but also valuable species-specific information. This information may include the complete taxonomic hierarchy of each species (such as class, order, family, etc.) or the IUCN red list category (such as endangered, near threatened, etc.). While often ignored, this fine-grained information could be incorporated to enhance the performance and

interpretability of SDMs. In this work, we incorporate the taxonomic hierarchy of species into our SDM in the form of text. Each species is uniquely identified by its taxonomic classification ranks, which are represented as key-value pairs. For instance, a key-value pair that represents the *wild duck* is shown below:

$t = \{\text{class: Aves, order: Anseriformes, family: Anatidae, genus: Anas, species: Anas platyrhynchos}\}$

Recently, Large Language Models (LLMs) have demonstrated excellent capabilities in representing implicit knowledge, linguistic structure, and hierarchical concepts when trained on massive amounts of data [1]. With no finetuning, pretrained LLMs have shown impressive zero-shot performance with zero in-domain data. In this work, we use the recently released, LLaMA-2 [42] to encode the species-specific key-value pairs as text. We experiment with three variants of LLaMA-2: 7B, 13B, and 70B.

3.4. Loss Functions

Our formulation of the SDM falls in the domain of multi-label long-tailed learning, where the model learns to predict the likelihood probability over *each* location for a given species. Since we are modeling the likelihood over locations, our problem differs from the Single Positive Multi Label (SPML) task [14]. Here, we are given multiple positive locations of occurrence for each species. We explore different types of losses for our models that do not require pseudo-negative sampling, such as ASL and RAL. However, for the state-of-the-art models, we use all types of losses, including AN-full and ME-full, thereby extending their work. We describe the losses in detail below.

Full Assume-Negative (AN-Full). This loss is a kind of pseudo-negative sampling multi-label learning loss based on the argument that the majority of the species are absent at any given location [15]. This is typically used in SPML problems. The loss is given by:

$$\mathcal{L}_{\text{AN-full}}(\hat{y}, y) = -\frac{1}{S} \sum_{s=1}^S [\mathbb{1}_{[y_s=1]} \alpha \log(\hat{y}_s) + \mathbb{1}_{[y_s=0]} \log(1 - \hat{y}_s) + \log(1 - \hat{r}_s)] \quad (1)$$

where \hat{r} is a uniformly randomly sampled location from the spatial domain of the globe.

Full Maximum-Entropy (ME-Full). This loss was introduced in [49] to solve SPML problems. The idea of this loss is to maximize the entropy of predictions for negative samples and for randomly sampled pseudo-negative samples.

The loss is given by:

$$\mathcal{L}_{\text{ME-full}}(\hat{y}, y) = -\frac{1}{S} \sum_{s=1}^S [\mathbb{1}_{[y_s=1]} \alpha \log(\hat{y}_s) + \mathbb{1}_{[y_s=0]} H(\hat{y}_s) + H(\hat{r}_s)] \quad (2)$$

$$H(\hat{y}) = -[\hat{y} \log(\hat{y}) + (1 - \hat{y}) \log(1 - \hat{y})]$$

where again \hat{r} is a uniformly randomly sampled location.

Asymmetric Loss (ASL). This loss, proposed by [32], weights positive and negative samples differently. The positive and hard negative samples are given more weight. It is a fairly general loss for multi-label learning which can also be used for SPML, without the need for pseudo-negative sampling. This loss is given by:

$$\mathcal{L}_{\text{ASL}}(\hat{y}, y) = -\frac{1}{S} \sum_{s=1}^S [\mathbb{1}_{[y_s=1]} (1 - \hat{y}_s)^{\gamma^+} \log(\hat{y}_s) + \mathbb{1}_{[y_s=0]} (p_s^\tau)^{\gamma^-} \log(1 - p_s^\tau)] \quad (3)$$

where $p^\tau = \max(\hat{y} - \tau)$ is used for hard thresholding easy negatives.

Robust Asymmetric Loss (RAL). Recently, [31] proposed an improved version of the ASL loss by combining the Asymmetric Polynomial Loss (APL) [21] and the Hill loss [48], which makes it less sensitive to hyperparameters. This loss is given by:

$$\mathcal{L}_{\text{RAL}}(\hat{y}_s, y_s) = \left[\sum_{m=1}^M \mathbb{1}_{[y_s=1]} \alpha_m (1 - \hat{y}_s)^{m+\gamma^+} + \sum_{n=1}^N \mathbb{1}_{[y_s=0]} \psi(\hat{y}_s) \beta_n (p_s^\tau)^{n+\gamma^-} \right] \quad (4)$$

where $\psi(\hat{y}_s) = \lambda - \hat{y}_s$ is the Hill loss term. M , N , α_n and β_n are balance parameters for positive and negative samples.

4. Experiments

In this section, we describe the implementation details and performance of our models compared to the state-of-the-art models on the task of species range prediction and geo-feature regression.

4.1. Implementation Details

As described in section 3.2, we use SFNO to extract geographic and environmental-specific features. The architecture is borrowed from [5]. We use two spectral and encoder layers in the SFNO. The encoder dimension used is 128 while the number of SFNO blocks are two. For the

coordinate-only models, we drop the environmental features during the training. For the text encoder, we use *frozen* LLaMA-2 [42] (70B variant) and extract its encoder outputs for each species. Before training, we precompute and save the embeddings for each species in the disk. For the multi-label classifier, we use a single-layer multi-headed cross-attention network followed by a fully-connected layer with sigmoid activations. We compare LD-SDM with two state-of-art-models: SINR [15] and SIREN(SH) [34]. SINR learns an end-to-end neural representation of geographic locations that is used to predict the likelihood over species. SIREN(SH) uses a spherical harmonic representation of geographic locations which is then used to predict the likelihood over species. The rest of the details about our models and the implementation of state-of-the-art models are described in Appendix C.

4.2. Proximity-Aware Evaluation

Evaluating SDMs is a challenging task since it requires the comparison of spatially distributed probability values. Pixel-wise comparison methods are not well-suited for this task since they are susceptible to spatial prediction shifts. Intuitively, false positive predictions that are geographically distant from true positive predictions are more significant than those that are close. This is not inherent in the evaluation metrics used by previous studies such as the Kullback–Leibler divergence, AUC, or MAP, which are invariant of the spatial arrangement of probability mass.

A well-known spatially explicit distance used for comparing any two distributions is the Earth-Mover (Wasserstein) Distance. Due to its computational requirements and infeasibility on large-scale data points, Chamfer Distance is a popularly used proxy [3]. However, it has only been developed for point clouds and there doesn’t exist a chamfer distance measure to compare two spatial probability distributions. Inspired by [46], we make a simple modification to their Density-Aware Chamfer Distance (DCD) metric that works for comparing a *predicted* probability distribution map (P_1) with a *binary* probability map (P_2) representing the ground truth. We add a likelihood probability term which weights the distance term. We call this metric One-Way Probability Weighted Chamfer Distance (PWCD), which measures the false positive rate in a proximity-aware manner. This metric is between [0,1] and could also be used to compute the number of false positives instead of the rate. It is given by:

$$d_{PWCD}(P_1, P_2) = \frac{1}{|N|} \sum_{x \in P_1} \left(1 - e^{-\alpha p(x) \|x-y\|_2}\right) \quad (5)$$

$$FP_{PWCD}(P_1, P_2) = \sum_{x \in P_1} \left(1 - e^{-\alpha p(x) \|x-y\|_2}\right) \quad (6)$$

where, $y = \underset{z \in P_2 \cap p(z)=1}{\operatorname{argmin}} \|x-z\|_2$. This represents the near-

est neighbor ground-truth observation of a given pixel x in the predicted probability distribution map. $N = \{z \in P_2 | p(z) = 0\}$ is the set of all negative observations in the ground truth. α is a temperature parameter that controls the exponential weighting of the distance. See Appendix B for more details. For our case, $|P_1| = |P_2| = L$. Notice that we have omitted the density term in the metric as our probability maps are a contiguous grid of pixels and equally dense everywhere. Since it is a proxy for false positives, it can be plugged into any other metric of choice such as the MAP and AUC. In this work, we report proximity-adjusted MAP scores denoted as MAP(pa) by replacing false positives with our metric. All the scores reported are an average over scores computed for each species category.

4.3. Training and Evaluation

We focus on bird species occurrence data which is abundantly available yet challenging to model as compared to other species due to complex migration patterns. We compiled 131.7 million observations of 4141 species of birds using the GBIF (gbif.org) platform which includes data from various community science platforms. This data is collected for the years 2012-2020. For evaluation, we use curated research-grade observations from the iNaturalist [44] and eBird [37] for 2021 and 2022. These contain 17.9 million and 17.2 million observations respectively. Using the same platform, we created a dataset of 84 species that are unseen (not present in training data) and rare (< 1000 observations) for zero-shot performance evaluation. This contains a total of 26k observations. These platforms are useful since errors in misclassification are highly mitigated due to community consensus [24], hence being a strong representative of the ground truth. Further, we use the same procedure as described in [15] for the geo-feature regression task.

All the training and evaluations are done at a spatial resolution of 0.2° . This implies $L = 1,620,000$. During training, we create ground-truth pixel-level range maps for each species at 0.2° resolution using the observations present in the occurrence data. For this, we use the histogram binning technique and clip all the values greater than one to one [15]. These maps are then used to calculate the various multi-label learning losses described previously. Finally, we report MAP(pa) and d_{PWCD} using $\alpha = 0.1$ for the species range prediction task and R^2 for the geo-feature regression task. See Appendix C for more details on the training settings and hyperparameters used.

4.4. Results

Quantitative Evaluation. In Table 1, we report the performance of all the models considered in this work. LD-SDM has shown better performance than the other models on the task of species range prediction. The zero-shot

Table 1. Comparison of performance of SDMs over a variety of multi-label learning losses on two tasks: species range prediction (and zero-shot range prediction) and geo-feature regression. The proximity-aware metrics proposed are defined in Section 4.2.

Loss	Env.	Method	GBIF'21		GBIF'22		Zero Shot		Geo Feature
			MAP(pa) \uparrow	d_{PWCD} \downarrow	MAP(pa) \uparrow	d_{PWCD} \downarrow	MAP(pa) \uparrow	d_{PWCD} \downarrow	(Mean R^2)
$\mathcal{L}_{AN-full}$ [15]	\times	SINR [15]	62.64	0.177	60.28	0.178	-	-	0.446
$\mathcal{L}_{ME-full}$ [49]	\times	SINR	61.88	0.189	58.81	0.187	-	-	0.518
\mathcal{L}_{ASL} [32]	\times	SINR	67.11	0.152	64.55	0.155	-	-	0.619
\mathcal{L}_{RAL} [31]	\times	SINR	62.02	0.291	60.42	0.297	-	-	0.536
$\mathcal{L}_{AN-full}$	\times	SIREN(SH) [34]	61.99	0.203	60.67	0.215	-	-	0.562
$\mathcal{L}_{ME-full}$	\times	SIREN(SH)	64.44	0.197	64.16	0.212	-	-	0.630
\mathcal{L}_{ASL}	\times	SIREN(SH)	62.56	0.189	62.43	0.206	-	-	0.481
\mathcal{L}_{RAL}	\times	SIREN(SH)	63.13	0.192	62.98	0.209	-	-	0.488
\mathcal{L}_{ASL}	\times	LD-SDM (ours)	73.88	0.174	71.45	0.182	59.27	0.648	0.583
\mathcal{L}_{RAL}	\times	LD-SDM (ours)	73.46	0.176	71.52	0.184	55.22	0.694	0.587
$\mathcal{L}_{AN-full}$	\checkmark	SINR	64.25	0.184	62.43	0.181	-	-	-
$\mathcal{L}_{ME-full}$	\checkmark	SINR	64.13	0.200	60.67	0.222	-	-	-
\mathcal{L}_{ASL}	\checkmark	SINR	67.23	0.172	69.49	0.179	-	-	-
\mathcal{L}_{RAL}	\checkmark	SINR	64.98	0.224	63.77	0.252	-	-	-
\mathcal{L}_{ASL}	\checkmark	LD-SDM (ours)	74.16	0.222	72.54	0.231	61.14	0.702	-
\mathcal{L}_{RAL}	\checkmark	LD-SDM (ours)	75.26	0.219	74.13	0.224	59.65	0.715	-

Table 2. Comparison of performance of our models using three different variants of LLaMA-2. The 70B variant achieves the best performance followed by the 7B and 13B variants.

Text Encoder	encoding dim	GBIF'21		GBIF'22		Zero Shot		Geo Feature	FLOPS
		MAP(pa) \uparrow	d_{PWCD} \downarrow	MAP(pa) \uparrow	d_{PWCD} \downarrow	MAP(pa) \uparrow	d_{PWCD} \downarrow	(Mean R^2)	TFLOPS
LLaMA-2-7B	4096	71.24	0.177	70.25	0.178	56.27	0.719	0.579	0.174
LLaMA-2-13B	5120	70.11	0.184	69.09	0.193	55.70	0.732	0.563	0.342
LLaMA-2-70B	8192	73.88	0.174	71.45	0.182	59.27	0.648	0.583	1.848

performance of LD-SDM on unseen species is reasonably good. Although it has an increased false-positive rate, it can be attributed to the model using higher-level taxonomic relationships. \mathcal{L}_{RAL} tends to produce overconfident predictions as noticeable from the high MAP(pa) scores corresponding to high d_{PWCD} scores (especially for SINR and SIREN(SH)). On average, \mathcal{L}_{ASL} loss is likely to be better performing than the other losses over all the models. For SINR, \mathcal{L}_{ASL} performs the best as compared to the other losses by a large margin. This is also evident in the geo-feature regression task. Our model has also produced competitive scores on the task of geo-feature regression. The coordinate-only models perform nearly as well as models incorporating environmental features. So, dropping environmental features could result in faster training times.

Qualitative Examples. In Figure 3, we show global-scale

species distribution maps generated for five bird species. To make fair comparisons, we used the best-performing coordinate-only models to ensure no bias is added into models from the environmental features. Although SINR and SIREN(SH) could generate species distribution maps at any spatial resolution, they tend to learn a very low-frequency function over the sphere as evident from the blob-like maps. SIREN(SH) produces a lot of false positive predictions possibly due to the limitation of the number of Legendre polynomials it can fit. Our model on the other hand learns to predict species ranges at a more fine-grained level. This is evident from the visualization of the geographic location features learned by the location encoder of each model (shown in Appendix D). Fine-grained geographic features are important for better geolocalization of species. SINR and SIREN(SH) tend to learn similar features over large geographic regions while LD-SDM produces higher variabil-

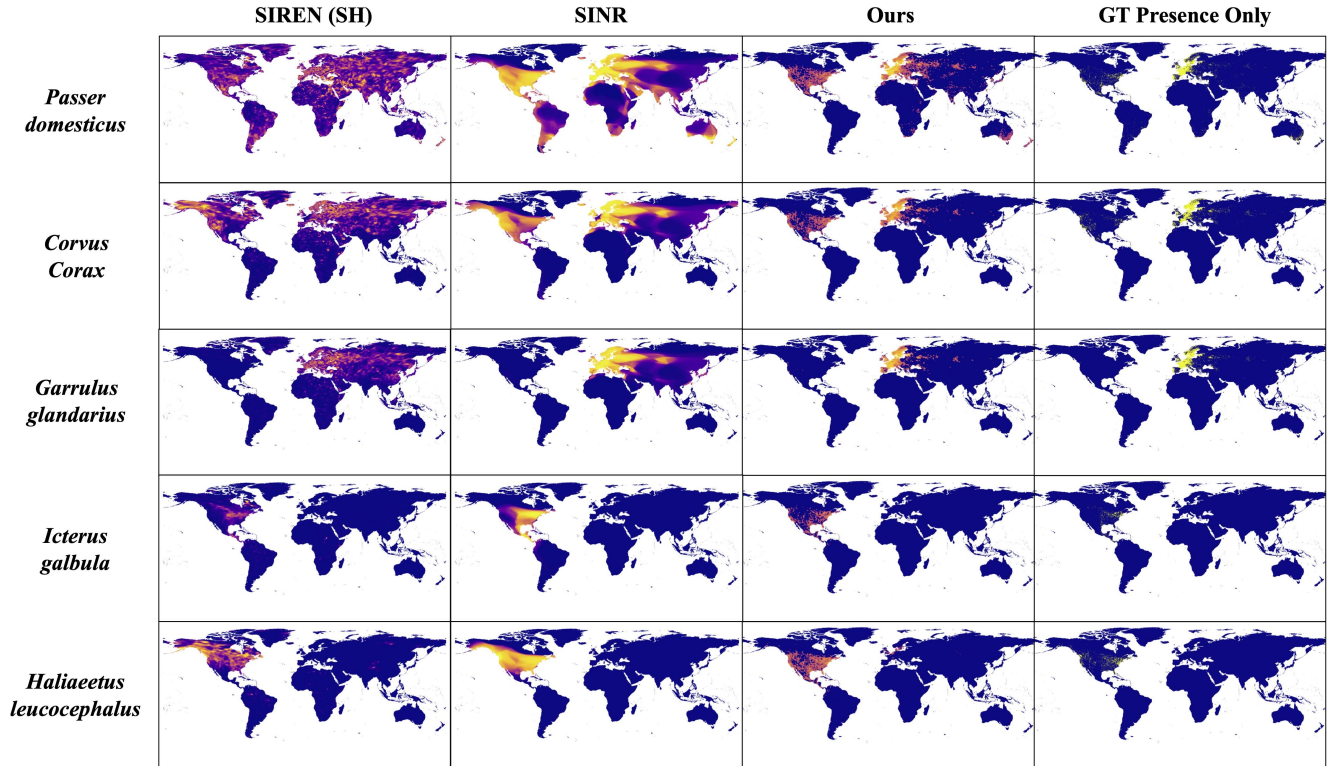


Figure 3. **Predicted Range Maps (Probability Values)**. The predictions are generated at a spatial resolution of 0.2 degrees. The best performing models are used in each case. For the SIREN(SH) and SINR models, predictions are generated at the center of each raster cell. The visualizations show that our model performs better than other models at resolving higher frequencies over the sphere and localizing the species distribution.

Table 3. Comparison of taxonomic mapping performance of our models using the three different variants of LLaMA-2 for taxonomic encoding. These performances are reported on the combined presence-only dataset from GBIF for the years 2012-2022. It is worth noting that LLaMA-2-13b has a lower performance than LLaMA-2-7b, possibly due to differences in their training data.

Taxonomic Level	LLaMA-2-7B		LLaMA-2-13B		LLaMA-2-70B	
	MAP(pa) \uparrow	d_{PWCD} \downarrow	MAP(pa) \uparrow	d_{PWCD} \downarrow	MAP(pa) \uparrow	d_{PWCD} \downarrow
Class	97.10	0.117	95.2	0.204	97.52	0.163
Order	56.15	0.450	55.94	0.472	58.31	0.414
Family	38.18	0.659	36.47	0.688	40.13	0.632
Genus	24.95	0.710	24.97	0.711	27.86	0.692

Table 4. Comparison of performance of three different backbones used in the parameterization network. All the models are trained with the same loss with environmental features included in the inputs.

Backbone	Params M	GBIF'21		GBIF'22	
		MAP(pa) \uparrow	d_{PWCD} \downarrow	MAP(pa) \uparrow	d_{PWCD} \downarrow
Segformer [47]	20.81	71.64	0.247	70.54	0.255
DINOv2 [30]	41.34	72.19	0.232	72.01	0.240
SFNO [5]	19.19	74.16	0.222	72.54	0.231

encoder dim	GBIF'21		GBIF'22		encoder layers	GBIF'21		GBIF'22	
	MAP(pa) ↑	d_{PWCD} ↓	MAP(pa) ↑	d_{PWCD} ↓		MAP(pa) ↑	PWCD ↓	MAP(pa) ↑	PWCD ↓
64	68.55	0.147	67.28	0.149	2	73.88	0.174	71.45	0.182
128	73.88	0.174	71.45	0.182	3	73.39	0.171	72.11	0.174
256	73.67	0.178	71.82	0.188	4	73.67	0.174	72.00	0.180

(a) SFNO width

(b) SFNO depth

Table 5. **SFNO ablation in LD-SDM.** All experiments run with the \mathcal{L}_{ASL} loss and the LLaMA-2-70B variant.

ity in the features at a finer scale.

Effect of LLaMA-2 variants on LD-SDM. We assess the impact of using different variants of LLaMA-2 for LD-SDM in Table 2. In particular, we compare the 7B, 13B, and 70B variants. Surprisingly, the 13B variant performs the worst. This is possibly due to the differences in the training data of the variants. Empirically, this can be explained by examining the T-SNE plots of text embeddings. In Appendix A, we present T-SNE plots along with mean intra-cluster and inter-cluster distances of text embeddings. Ideally, both intra-cluster and inter-cluster distances should be high to ensure separability within a particular taxonomic class and between taxonomic classes respectively. 13B variant has the poorest separability at every taxonomic rank. The 7B and 70B variants have almost identical separabilities. The impressive performance of the 70B variant can be attributed to its high dimensionality of the species-specific encoding. Although 70B has noticeably higher computational overheads, it is compensated by precomputing the text embeddings before training. Overall, all the variants are able to perform better than the state-of-the-art.

Taxonomic range mapping using LLaMA-2 variants. We perform range prediction over the taxonomic ranks: *class*, *order*, *family*, and *genus*. The procedure is the same as for generating species range maps. We precompute the embeddings for each rank as shown in Figure 1. The range map for the rank *class* represents the unconditional distribution of finding any bird *species* in the world. As one moves down in the hierarchy, the range maps become more and more fine-grained. As expected, the performance of LD-SDM drops as one moves down in the hierarchy (Table 3). This can be explained by examining the increasing d_{PWCD} scores. The T-SNE plots of the embeddings of various ranks in Appendix A help in better understanding the increase in false positive rates as one moves down in the hierarchy. As it can be seen, the intra-cluster distances decrease substantially when moving down in the hierarchy. As a result, it becomes challenging for the model to distinguish between birds for example of *genera* belonging to the same *family*. On the other hand, when training in a fully supervised manner at the *species* rank, the model is able to achieve impressive performance. This shows the importance of supervision in SDM.

Spherical Harmonics are important for SDM. We compare the performance of LD-SDM when using different backbones in the location encoder network (Table 4). All the models are trained from scratch using the LLaMA-2-70B variant. We use the same training inputs including the environmental features. All the models are trained using the \mathcal{L}_{ASL} loss. Notice that SFNO gives the best performance over Segformer and DINOv2. With SFNO, we observe a significant gain in performance and a reduction in false positives. Overall, a robust geographic feature extractor is beneficial for SDM and SFNO proves to be one such architecture.

Lightweight SFNO performs surprisingly well. In Table 5, we show the effect on the performance of species range prediction due to different components of the SFNO. It is noteworthy that an encoder dimension of 128 for SFNO yields results on par with an encoder dimension of 256 while reducing computational complexity. On the other hand, having fewer encoder layers in SFNO is beneficial since performance gain from adding additional encoder layers is marginal. In conclusion, a lightweight SFNO is a strong geographic feature extractor that can be used in various downstream global-scale geospatial tasks.

5. Conclusions

We introduced a novel approach for species distribution modeling that uses a large-language model to generate a representation of a species. This provides flexibility to generate distributions at different levels of the taxonomic hierarchy and for unseen species. In addition, we introduced a new evaluation metric, Probability Weighted Chamfer Distance. This metric computes the false positive rate in species range mapping tasks in a proximity-aware manner. While our focus was on species distribution modeling, the integration of large-language models points to some intriguing potential future use cases. It might be possible, for example, to generate distribution models from arbitrary text, such as “a large white bird” or “a flock of red-winged blackbirds”. This is potentially more useful for non-expert users. Finally, alternative text prompts could be explored as future work which may better reason about a species and its dependence on a particular geographic location.

References

- [1] Rohan Anil, Andrew M Dai, Orhan Firat, Melvin Johnson, Dmitry Lepikhin, Alexandre Passos, Siamak Shakeri, Emanuel Taropa, Paige Bailey, Zhifeng Chen, et al. Palm 2 technical report. *arXiv preprint arXiv:2305.10403*, 2023. 4
- [2] Kumar Ayush, Burak Uz Kent, Chenlin Meng, Kumar Tanmay, Marshall Burke, David Lobell, and Stefano Ermon. Geography-aware self-supervised learning. In *Proceedings of the IEEE/CVF International Conference on Computer Vision*, pages 10181–10190, 2021. 2
- [3] Ainesh Bakshi, Piotr Indyk, Rajesh Jayaram, Sandeep Silwal, and Erik Waingarten. A near-linear time algorithm for the chamfer distance. *arXiv preprint arXiv:2307.03043*, 2023. 5
- [4] Sara Beery, Elijah Cole, Joseph Parker, Pietro Perona, and Kevin Winner. Species distribution modeling for machine learning practitioners: A review. In *ACM SIGCAS conference on computing and sustainable societies*, pages 329–348, 2021. 2
- [5] Boris Bonev, Thorsten Kurth, Christian Hundt, Jaideep Pathak, Maximilian Baust, Karthik Kashinath, and Anima Anandkumar. Spherical fourier neural operators: Learning stable dynamics on the sphere. *International conference on machine learning*, 2023. 2, 3, 4, 7
- [6] Christophe Botella, Alexis Joly, Pierre Bonnet, Pascal Monestiez, and François Munoz. A deep learning approach to species distribution modelling. *Multimedia Tools and Applications for Environmental & Biodiversity Informatics*, pages 169–199, 2018. 2
- [7] Christophe Botella, Maximilien Servajean, Pierre Bonnet, and Alexis Joly. Overview of geolifeclef 2019: plant species prediction using environment and animal occurrences. In *CLEF 2019 Working Notes-Conference and Labs of the Evaluation Forum*, page 257, 2019. 2
- [8] Christophe Botella, Alexis Joly, Pierre Bonnet, François Munoz, and Pascal Monestiez. Jointly estimating spatial sampling effort and habitat suitability for multiple species from opportunistic presence-only data. *Methods in Ecology and Evolution*, 12(5):933–945, 2021. 2
- [9] Bogdan Caradima, Nele Schuwirth, and Peter Reichert. From individual to joint species distribution models: A comparison of model complexity and predictive performance. *Journal of Biogeography*, 46(10):2260–2274, 2019. 1
- [10] Di Chen and Carla P Gomes. Bias reduction via end-to-end shift learning: Application to citizen science. In *Proceedings of the AAAI Conference on Artificial Intelligence*, pages 493–500, 2019. 2
- [11] Di Chen, Yexiang Xue, Shuo Chen, Daniel Fink, and Carla Gomes. Deep multi-species embedding. *arXiv preprint arXiv:1609.09353*, 2016. 2
- [12] Grace Chu, Brian Potetz, Weijun Wang, Andrew Howard, Yang Song, Fernando Brucher, Thomas Leung, and Hartwig Adam. Geo-aware networks for fine-grained recognition. In *Proceedings of the IEEE/CVF International Conference on Computer Vision Workshops*, pages 0–0, 2019. 2
- [13] Elijah Cole, Benjamin Deneu, Titouan Lorieul, Maximilien Servajean, Christophe Botella, Dan Morris, Nebojsa Jojic, Pierre Bonnet, and Alexis Joly. The geolifeclef 2020 dataset. *arXiv preprint arXiv:2004.04192*, 2020. 2
- [14] Elijah Cole, Oisín Mac Aodha, Titouan Lorieul, Pietro Perona, Dan Morris, and Nebojsa Jojic. Multi-label learning from single positive labels. In *Proceedings of the IEEE/CVF Conference on Computer Vision and Pattern Recognition*, pages 933–942, 2021. 4
- [15] Elijah Cole, Grant Van Horn, Christian Lange, Alexander Shepard, Patrick Leary, Pietro Perona, Scott Loarie, and Oisín Mac Aodha. Spatial implicit neural representations for global-scale species mapping. *International conference on machine learning*, 2023. 1, 2, 3, 4, 5, 6, 7
- [16] Jane Elith and John R Leathwick. Species distribution models: ecological explanation and prediction across space and time. *Annual review of ecology, evolution, and systematics*, 40:677–697, 2009. 2
- [17] Jane Elith*, Catherine H. Graham*, Robert P. Anderson, Miroslav Dudík, Simon Ferrier, Antoine Guisan, Robert J. Hijmans, Falk Huettmann, John R. Leathwick, Anthony Lehmann, et al. Novel methods improve prediction of species’ distributions from occurrence data. *Ecography*, 29(2):129–151, 2006. 2
- [18] Stephen E Fick and Robert J Hijmans. Worldclim 2: new 1-km spatial resolution climate surfaces for global land areas. *International journal of climatology*, 37(12):4302–4315, 2017. 6
- [19] Daniel Fink, Wesley M Hochachka, Benjamin Zuckerberg, David W Winkler, Ben Shaby, M Arthur Munson, Giles Hooker, Mirek Riedewald, Daniel Sheldon, and Steve Kelling. Spatiotemporal exploratory models for broad-scale survey data. *Ecological Applications*, 20(8):2131–2147, 2010. 2
- [20] Simone Franceschini, Emanuele Gandola, Marco Martinoli, Lorenzo Tancioni, and Michele Scardi. Cascaded neural networks improving fish species prediction accuracy: the role of the biotic information. *Scientific Reports*, 8(1):4581, 2018. 2
- [21] Yusheng Huang, Jiexing Qi, Xinbing Wang, and Zhouhan Lin. Asymmetric polynomial loss for multi-label classification. In *ICASSP 2023-2023 IEEE International Conference on Acoustics, Speech and Signal Processing (ICASSP)*, pages 1–5. IEEE, 2023. 4, 7
- [22] Alison Johnston, Nick Moran, Andy Musgrove, Daniel Fink, and Stephen R Baillie. Estimating species distributions from spatially biased citizen science data. *Ecological Modelling*, 422:108927, 2020. 2
- [23] Kamil Konowalik and Agata Nosol. Evaluation metrics and validation of presence-only species distribution models based on distributional maps with varying coverage. *Scientific Reports*, 11(1):1482, 2021. 2
- [24] Christian Lange, Elijah Cole, Grant Van Horn, and Oisín Mac Aodha. Active learning-based species range estimation. *Advances in Neural Information Processing Systems*, 2023. 1, 3, 5
- [25] Titouan Lorieul, Elijah Cole, Benjamin Deneu, Maximilien Servajean, Pierre Bonnet, and Alexis Joly. Overview of geolifeclef 2021: Predicting species distribution from 2 million

- remote sensing images. In *CLEF (Working Notes)*, pages 1451–1462, 2021. [2](#)
- [26] Titouan Lorieul, Elijah Cole, Benjamin Deneu, Maximilien Servajean, Pierre Bonnet, and Alexis Joly. Overview of geolifeclef 2022: Predicting species presence from multi-modal remote sensing, bioclimatic and pedologic data. In *CLEF 2022-Conference and Labs of the Evaluation Forum*, pages 1940–1956, 2022. [2](#)
- [27] Oisín Mac Aodha, Elijah Cole, and Pietro Perona. Presence-only geographical priors for fine-grained image classification. In *Proceedings of the IEEE/CVF International Conference on Computer Vision*, pages 9596–9606, 2019. [1](#), [2](#), [3](#)
- [28] DARRYL I MacKENZIE. What are the issues with presence-absence data for wildlife managers? *The Journal of Wildlife Management*, 69(3):849–860, 2005. [2](#)
- [29] Anna Norberg, Nerea Abrego, F Guillaume Blanchet, Frederick R Adler, Barbara J Anderson, Jani Anttila, Miguel B Araújo, Tad Dallas, David Dunson, Jane Elith, et al. A comprehensive evaluation of predictive performance of 33 species distribution models at species and community levels. *Ecological monographs*, 89(3):e01370, 2019. [2](#)
- [30] Maxime Oquab, Timothée Darcet, Théo Moutakanni, Huy Vo, Marc Szafraniec, Vasil Khalidov, Pierre Fernandez, Daniel Haziza, Francisco Massa, Alaaeldin El-Nouby, et al. Dinov2: Learning robust visual features without supervision. *arXiv preprint arXiv:2304.07193*, 2023. [7](#)
- [31] Wongi Park, Inhyuk Park, Sungeun Kim, and Jongbin Ryu. Robust asymmetric loss for multi-label long-tailed learning. *arXiv preprint arXiv:2308.05542*, 2023. [2](#), [4](#), [6](#)
- [32] Tal Ridnik, Emanuel Ben-Baruch, Nadav Zamir, Asaf Noy, Itamar Friedman, Matan Protter, and Lihi Zelnik-Manor. Asymmetric loss for multi-label classification. In *Proceedings of the IEEE/CVF International Conference on Computer Vision*, pages 82–91, 2021. [2](#), [4](#), [6](#), [7](#)
- [33] Tim Robertson, Markus Döring, Robert Guralnick, David Bloom, John Wieczorek, Kyle Braak, Javier Otegui, Laura Russell, and Peter Desmet. The gbif integrated publishing toolkit: facilitating the efficient publishing of biodiversity data on the internet. *PLoS one*, 9(8):e102623, 2014. [5](#)
- [34] Marc Rußwurm, Konstantin Klemmer, Esther Rolf, Robin Zbinden, and Devis Tuia. Geographic location encoding with spherical harmonics and sinusoidal representation networks. *arXiv preprint arXiv:2310.06743*, 2023. [2](#), [5](#), [6](#)
- [35] Srikumar Sastry, Subash Khanal, Aayush Dhakal, Di Huang, and Nathan Jacobs. Birdsat: Cross-view contrastive masked autoencoders for bird species classification and mapping. *IEEE/CVF Winter Conference on Applications of Computer Vision*, 2024. [2](#), [3](#)
- [36] Pedro Segurado and Miguel B Araújo. An evaluation of methods for modelling species distributions. *Journal of biogeography*, 31(10):1555–1568, 2004. [2](#)
- [37] Brian L Sullivan, Christopher L Wood, Marshall J Iliff, Rick E Bonney, Daniel Fink, and Steve Kelling. ebird: A citizen-based bird observation network in the biological sciences. *Biological conservation*, 142(10):2282–2292, 2009. [5](#)
- [38] Luming Tang, Yexiang Xue, Di Chen, and Carla Gomes. Multi-entity dependence learning with rich context via conditional variational auto-encoder. In *Proceedings of the AAAI conference on artificial intelligence*, 2018. [2](#)
- [39] Mélisande Teng, Amna Elmustafa, Benjamin Akera, Yoshua Bengio, Hager Radi Abdelwahed, Hugo Larochelle, and David Rolnick. Satbird: Bird species distribution modeling with remote sensing and citizen science data. *Advances in Neural Information Processing Systems*, 2023. [2](#), [3](#)
- [40] Mélisande Teng, Amna Elmustafa, Benjamin Akera, Hugo Larochelle, and David Rolnick. Bird distribution modelling using remote sensing and citizen science data. *arXiv preprint arXiv:2305.01079*, 2023. [2](#)
- [41] James T Thorson, James N Ianello, Elise A Larsen, Leslie Ries, Mark D Scheuerell, Cody Szuwalski, and Elise F Zipkin. Joint dynamic species distribution models: a tool for community ordination and spatio-temporal monitoring. *Global Ecology and Biogeography*, 25(9):1144–1158, 2016. [1](#)
- [42] Hugo Touvron, Louis Martin, Kevin Stone, Peter Albert, Amjad Almahairi, Yasmine Babaei, Nikolay Bashlykov, Soumya Batra, Prajjwal Bhargava, Shruti Bhosale, et al. Llama 2: Open foundation and fine-tuned chat models. *arXiv preprint arXiv:2307.09288*, 2023. [4](#), [5](#)
- [43] Roozbeh Valavi, Gurutzeta Guillera-Arroita, José J Lahoz-Monfort, and Jane Elith. Predictive performance of presence-only species distribution models: a benchmark study with reproducible code. *Ecological Monographs*, 92(1):e01486, 2022. [2](#)
- [44] Grant Van Horn, Oisín Mac Aodha, Yang Song, Yin Cui, Chen Sun, Alex Shepard, Hartwig Adam, Pietro Perona, and Serge Belongie. The inaturalist species classification and detection dataset. In *Proceedings of the IEEE conference on computer vision and pattern recognition*, pages 8769–8778, 2018. [3](#), [5](#)
- [45] Peter D Wilson. Distance-based methods for the analysis of maps produced by species distribution models. *Methods in Ecology and Evolution*, 2(6):623–633, 2011. [2](#)
- [46] Tong Wu, Liang Pan, Junzhe Zhang, Tai Wang, Ziwei Liu, and Dahua Lin. Density-aware chamfer distance as a comprehensive metric for point cloud completion. *Advances in Neural Information Processing Systems*, 2021. [5](#)
- [47] Enze Xie, Wenhui Wang, Zhiding Yu, Anima Anandkumar, Jose M Alvarez, and Ping Luo. Segformer: Simple and efficient design for semantic segmentation with transformers. *Advances in Neural Information Processing Systems*, 34:12077–12090, 2021. [7](#)
- [48] Youcai Zhang, Yuhao Cheng, Xinyu Huang, Fei Wen, Rui Feng, Yaqian Li, and Yandong Guo. Simple and robust loss design for multi-label learning with missing labels. *arXiv preprint arXiv:2112.07368*, 2021. [2](#), [4](#)
- [49] Donghao Zhou, Pengfei Chen, Qiong Wang, Guangyong Chen, and Pheng-Ann Heng. Acknowledging the unknown for multi-label learning with single positive labels. In *European Conference on Computer Vision*, pages 423–440. Springer, 2022. [2](#), [4](#), [6](#)

LD-SDM: Language-Driven Hierarchical Species Distribution Modeling

Supplementary Material

A. Species-Specific Embeddings

As described in the paper, we encode the taxonomic information of species in the form of text. Text is a dictionary consisting of key-value pairs representing each taxonomic rank. We use `hugging-face`'s library `transformers` to obtain all the LLaMA-2 variants used in the paper. We separately compute and save the embeddings of the key-value pairs for each variant. In Table 6, we report the number of tokens generated by the LLaMA-2 variants for each taxonomic rank.

Table 6. Total tokens generated by LLaMA-2 for each taxonomic rank. The dimensionality of each of these tokens depends on the type of LLaMA-2 variant used.

Taxonomic Rank	#tokens	#classes	#total tokens
order	13	40	520
family	19	211	4009
genus	25	1393	34,825
species	34	4141	140,794

We create T-SNE plots in 2-D for visualizing the embeddings at each rank resulting from the variants (Figure 4). To create the plot, we do an average pool across the number of tokens' dimension for each text embedding. We then use `scikit-learn` library to compute the T-SNE embeddings for each species and at every taxonomic rank. We color code the embeddings based on the taxonomic rank one level higher than the current rank. For example, the T-SNE embeddings for the rank *family* are color-coded by their *order*. Doing this provides a simple intuition for interpreting the separability of species and taxonomic ranks.

We compute average inter-cluster and intra-cluster distances based on the color coding for each taxonomic rank. This is also done using the `scikit-learn` package. The inter-cluster distance represents the average dissimilarity between *species* (or any other rank) of different classes. The intra-cluster distance represents the average dissimilarity between *species* (or any other rank) of the same class. Intuitively, both distances should be high enough to ensure good separability for SDM. As we see, the distances decrease as we move down in the hierarchy. This is expected since the distribution of each species becomes more and more fine-grained. The 13B variant has abruptly low distances compared to the other variants suggesting poor performance in SDM. This can possibly be due to differences in training data and the training procedure between the variants.

B. Probability Weighted Chamfer Distance

We proposed the Probability Weighted Chamfer Distance (PWCD) which is a spatially-aware proxy for false-positive rates when comparing two probability maps. This distance could also be used in other metrics such as precision, MAP, or AUC to make them spatially aware. In Listing 1, we describe NumPy-style pseudocode for computing this distance metric.

Listing 1. NumPy-style pseudocode for computing d_{PWCD}

```
import xarray as xr
from xrspatial import proximity
import numpy as np

#y_true[h, w]: true binary range map
#y_pred[h, w]: predicted range map
#a: temperature parameter

def PWCD(y_true, y_pred, a):
    xr_true = xr.DataArray(y_true)
    prox_agg = np.array(proximity(xr_true))
    pwcd = 1 - np.exp(-a*y_pred*prox_agg)
    fps = np.sum(pwcd)
    neg = np.sum(y_true == 0)
    return fps / neg
```

We use the `xrspatial`'s `proximity` function for computing the nearest-neighbor distance map given the binary ground-truth range map. All the distances are measured in pixel units using Euclidean distance. The minimum possible distance is 0 which is for the positive pixels having *species* presence. The maximum possible distance depends on the spatial resolution of the range map. In our case, the spatial resolution of 0.2° gives a maximum distance of 2012.46. It is noteworthy that this distance function could be replaced with any other distance function for example the haversine distance.

We visualized the pixel-level d_{PWCD} map in Figure 5. Notice that the predictions spatially close to the true presence of *species* are weighted less than the predictions that are distant. This weighting is due to the nearest-neighbor distances of the pixels making the metric spatially-aware. The chamfer distance map describes the weighting of predictions as a function of distance from the nearest presence pixel. The weight gradually increases as the distance from the nearest presence pixel increases. Note that the nearest-neighbor distance map differs from the chamfer distance map, which is in the range of $[0,1]$. The chamfer distance map is computed using the nearest-neighbor distance map,

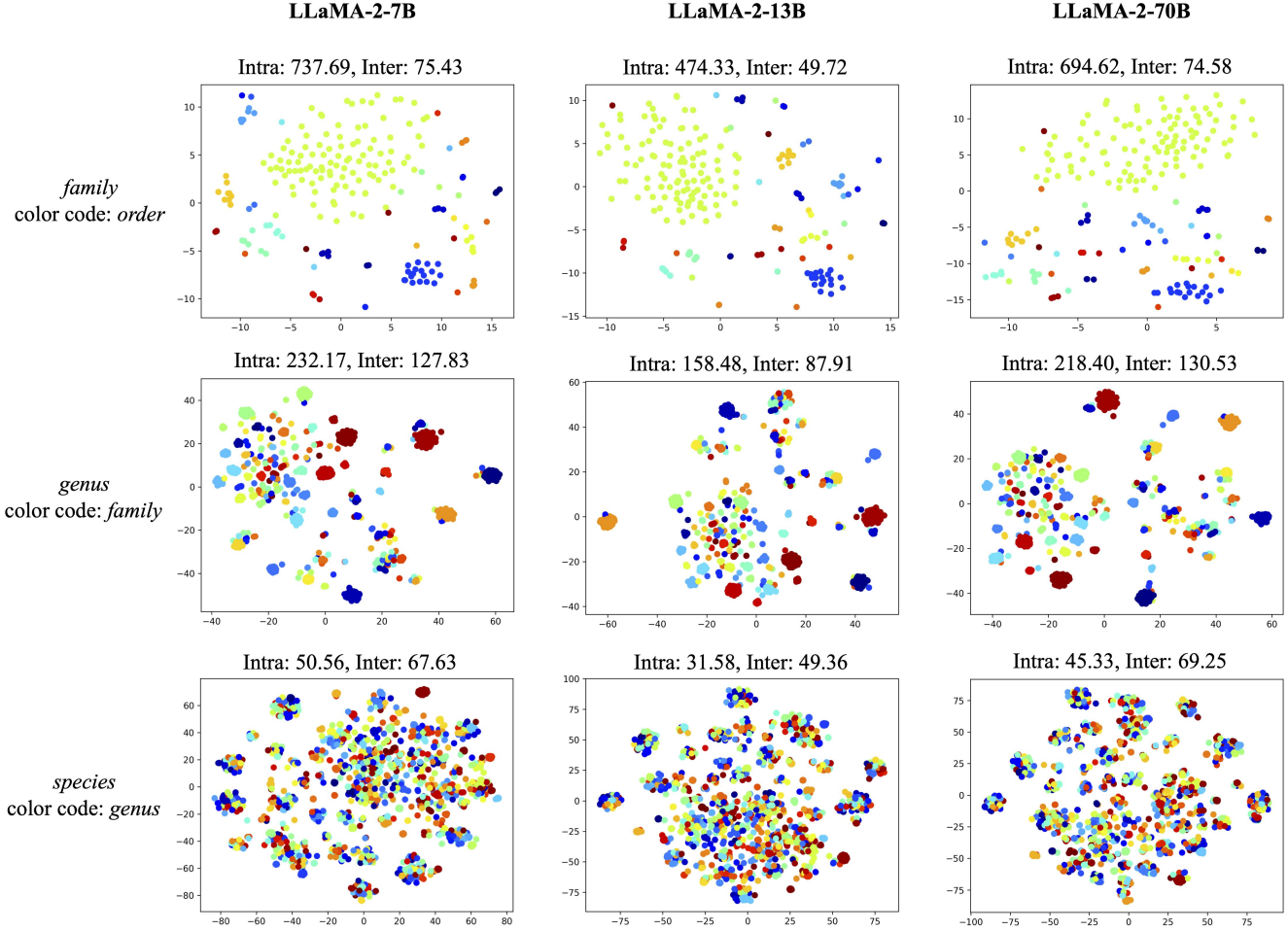


Figure 4. **T-SNE Plots of Text Embeddings.** For each variant and taxonomic rank, we compute the T-SNE embeddings of all the text tokens generated. We do average pooling over the token dimension before computing T-SNE. These plots highlight the separability degree of each variant over each taxonomic rank.

using the formula for d_{PWCD} and a constant likelihood term equal to one.

In Figure 6, we show the effect of temperature parameter α on the d_{PWCD} metric. The figure shows chamfer distance as a function of nearest-neighbor distance at a fixed likelihood probability of one and varying values of α . The parameter α controls the exponential weighting of the nearest-neighbor distance in the metric. Increasing α gradually increases the weight of nearby pixels. The metric starts penalizing more of the nearby pixels in the computation of false positive rates. A large value of α will make the metric more sensitive to spatial shifts in the predictions while a lower value of α will be more robust towards spatial shifts. However, an extremely low value of α will make the metric ignore distant false positives. As a result, an optimal value of α is essential to evaluate SDMs.

In order to evaluate the localization of species distributions, we have plotted d_{PWCD} scores with varying α in Fig-

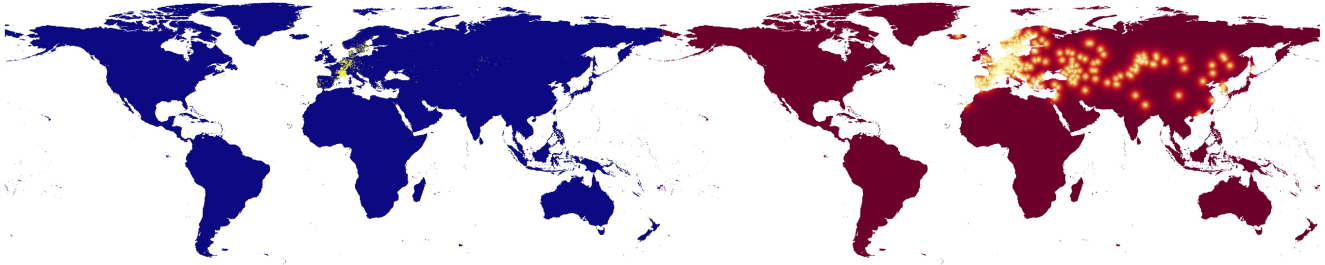
ure 7. The first plot shows the relationship between d_{PWCD} and the nearest neighbor distance for varying α values. By analyzing this graph, one can determine the optimal value of α for their specific application. For our purposes, we selected $\alpha = 0.1$, as it is robust to spatial shifts and accurately detects the distribution of species.

In the second plot, we have shown the d_{PWCD} scores as a function of the likelihood probability, at a constant nearest neighbor distance of 100 pixels. As the value of α increases, the metric starts penalizing low likelihood values. This gives us more control over the trade-off between the distance and likelihood scores, allowing us to determine the optimal α value for our application.

C. Training

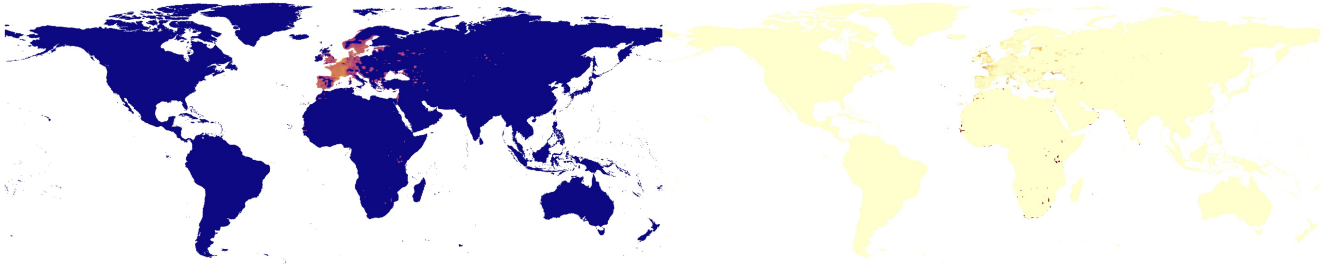
Below we describe the details of the datasets used. We also describe the implementation details of the models and the

Eurasian eagle-owl (*Bubo bubo*)



(a) GT Presence Only

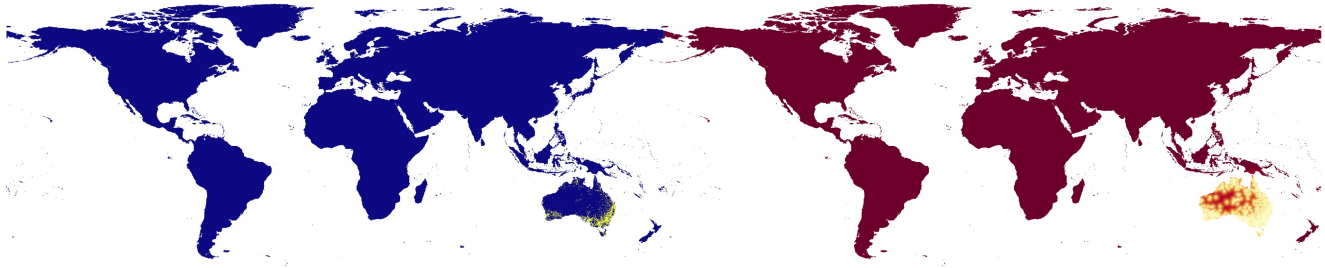
(b) Chamfer Distance



(c) Species Range Prediction

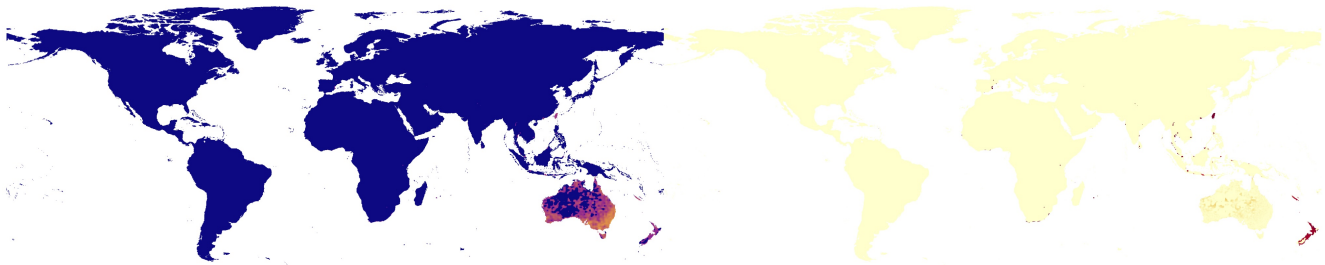
(d) Per-Pixel d_{pWCD} Metric

Striated Pardalote (*Pardalotus striatus*)



(a) GT Presence Only

(b) Chamfer Distance



(c) Species Range Prediction

(d) Per-Pixel d_{pWCD} Metric



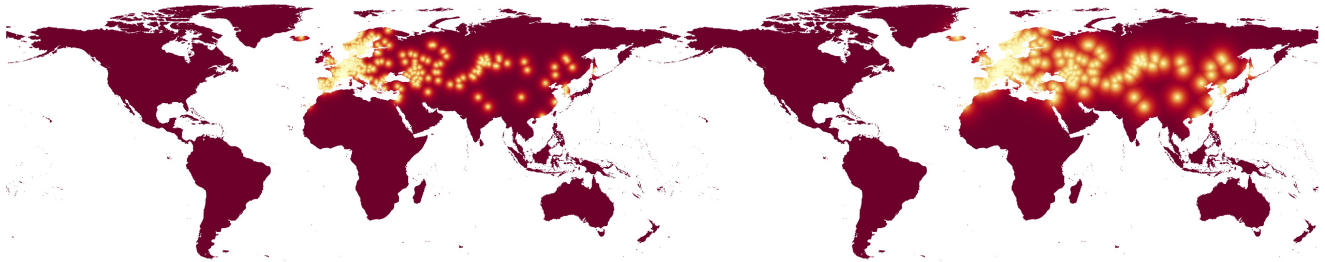
Figure 5. **Probability Weighted Chamfer Distance.** Using the presence-only ground-truth maps, the nearest-neighbor distance map is computed. Finally, d_{pWCD} is calculated using the per-pixel activation values from the range map predicted by an SDM and the nearest-neighbor distance map. The distance metric for computing the nearest-neighbor distance map is the Euclidean Distance in pixel units.

Eurasian eagle-owl (*Bubo bubo*)



(a) $\alpha = 1$

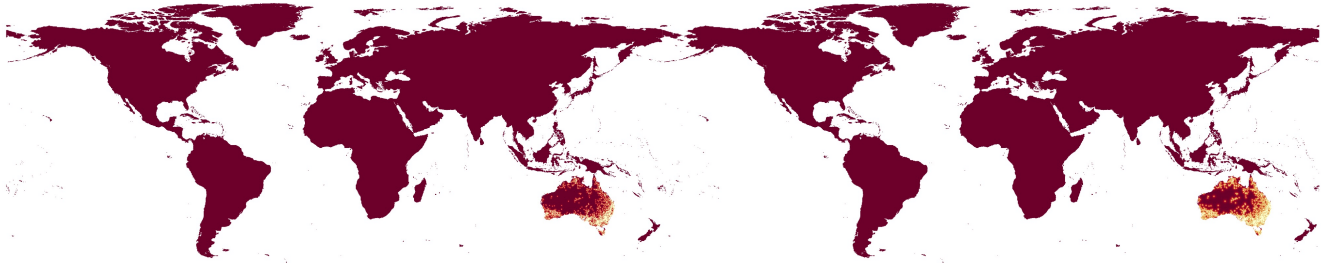
(b) $\alpha = 0.5$



(c) $\alpha = 0.1$

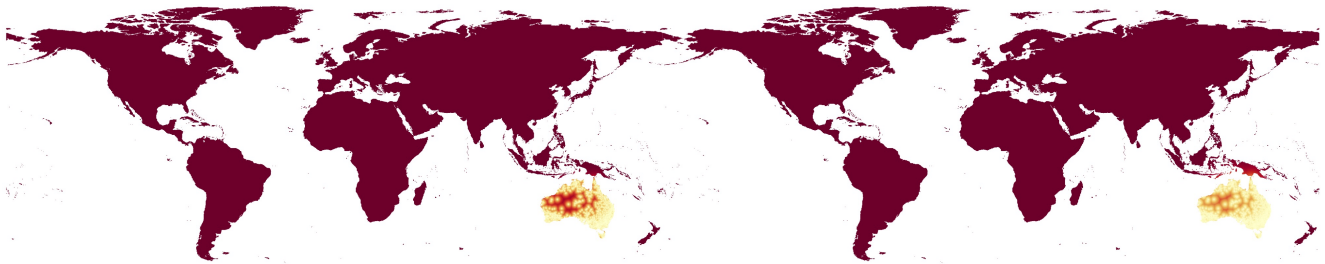
(d) $\alpha = 0.05$

Striated Pardalote (*Pardalotus striatus*)



(a) $\alpha = 1$

(b) $\alpha = 0.5$



(c) $\alpha = 0.1$

(d) $\alpha = 0.05$

Chamfer Distance



0.0

1.0

Figure 6. **Effect of α on Chamfer Distance.** With an increasing value of α , metric d_{PWCD} becomes more sensitive to prediction shifts. Lower values of α make the metric d_{PWCD} more robust to shifts at the cost of losing assessing spatial localizability in an effective sense.

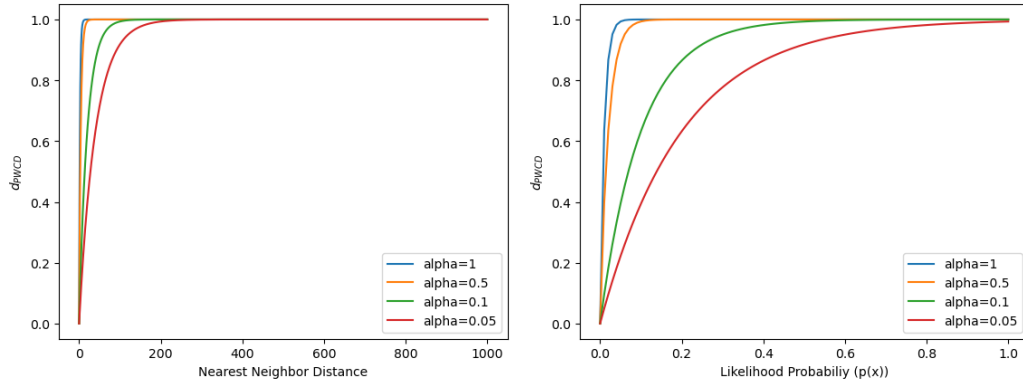


Figure 7. **Sensitivity of d_{PWCD} .** We show the variation of d_{PWCD} as distance to ground truth observation increases (left). We also show the variation of d_{PWCD} with likelihood probability at a fixed distance of 100 pixels from ground-truth (right).



(a) Training Observations (2012-2020)



(b) Testing Observations (2021)



(c) Testing Observations (2022)



(d) Unseen Species (2021-2022)

Figure 8. **Histogram of Locations of Observations.** We show the visualization of observations of the datasets considered in this study at a spatial resolution of 0.2° .

losses. Each training run was done on a single NVIDIA A40 GPU.

C.1. Data

Our training and evaluation data was collected using various citizen science platforms such as the iNaturalist ([inaturalist.org](https://www.inaturalist.org)) [44] and eBird (ebird.org) [37]. The maps in Figure 8 display the geographical locations of the observations

for each dataset across the globe. They were compiled using the GBIF (gbif.org) [33] platform, which hosts occurrence records of species from several citizen science platforms. For compilation, we used the following conditions:

1. All observations must have valid labels for each taxonomic rank and geographical location values.
2. All observations must have the *research grade* status label.

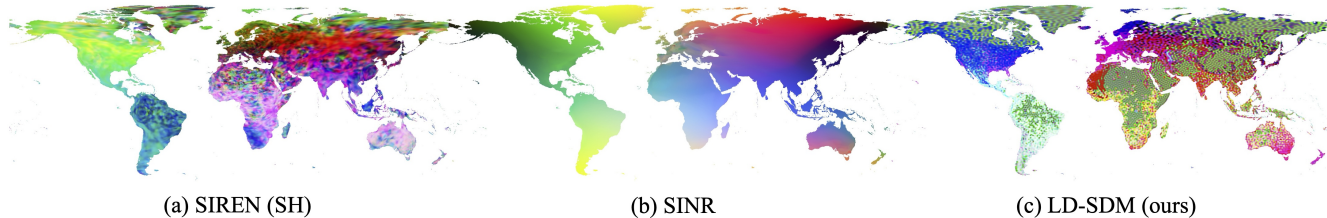


Figure 9. **Features Learned by Location Encoder.** We show the visualization of location embeddings learned by the location encoder of various models. For visualization, the embeddings are projected to a 3-dimensional space using Independent Component Analysis. SINR learns a low-frequency representation of location while SIREN(SH) and LD-SDM learn to localize at a fine-grained level.

To avoid bias, we excluded species with less than 100 observations. The evaluation datasets only contain observations from iNaturalist and eBird. For zero-shot evaluation, we selected the species that were not present in the training dataset. Further, we filtered out species with more than 1000 observations to focus on rare species. Table 7 shows the details of each dataset.

Table 7. Number of observations in each dataset compiled in this work.

Dataset	Year	#Observations	#species
Train	2012-2020	131.7M	4141
Test	2021	17.9M	3960
Test	2022	17.2M	4010
Zero-Shot	2021-2022	26k	84

We use bioclimatic variables and elevation data as environmental covariates in the SDM. The variables are derived from the WorldClim dataset (worldclim.org) [18], which are at a spatial resolution of 0.01° . The dataset is resampled to 0.2° resolution using bilinear interpolation. In total, the dataset contains 20 different variables (channels). We use nine different geographic features in the geo-feature regression task as done by [15]. These include above-ground carbon, elevation, etc. All the features are resampled to 0.2° resolution.

Table 8. Training settings for SINR

Config	Value
backbone	ResNet-style MLP
encoding dim	256
depth	4
input encoding	sin-cos
optimizer	AdamW
base learning rate	$5e-4$
learning rate scheduler	exponential decay
batch size	2048
epochs	10

Table 9. Training settings for SIREN(SH)

Config	Value
backbone	SIREN
encoding dim	256
depth	4
input encoding	spherical-harmonics
L	20
optimizer	AdamW
base learning rate	$1e-4$
learning rate scheduler	exponential decay
batch size	2048
epochs	20

Table 10. Training settings for LD-SDM

Config	Value
backbone	SFNO
encoding dim	128
SFNO blocks	2
multi-label classifier	hidden_dim: 64 num_heads: 16
optimizer	AdamW
base learning rate	$1e-5$
batch size	1
accumulate grad batches	64
epochs	10

C.2. Models

We experimented with three different SDMs: 1) SINR [15]; 2) SIREN(SH) [34]; LD-SDM (ours). For the baseline models, we used the same hyperparameters as reported by authors. Tables 8, 9 and 10, show the hyperparameters used for each model. We use $L = 20$ for SIREN(SH) since experiments with larger L were computationally infeasible.

C.3. Losses

We evaluated four different multi-label learning losses in our experiments, namely: 1) AN-full [15]; 2) ME-full [49];

3) ASL [32]; 4) RAL [21]. For AN-full and ME-full, we used a positive weight of 2048. The pseudo-negative sampling is done according to [15], by using a spherical buffer around each observation. In the case of ASL and RAL, we used 0 and 4 for γ^+ and γ^- respectively. In RAL, we set λ to 1.5.

D. Location Embeddings

We present the location-specific features learned by the SDMs in Figure 9. The location embeddings displayed are the output of the location encoder network for each SDM. We use Independent Component Analysis (ICA) to project the high-dimensional embeddings to a 3-dimensional space. All the maps are generated at a spatial resolution of 0.2° . SINR produces a smooth map indicating that it has failed to learn high-frequency functions. SIREN(SH) produces noisy location features spread across the globe. LD-SDM produces a map that resembles the distribution of training data. We see that in the locations where observations are absent, LD-SDM has learned similar features.

E. Limitations

As pointed out in [15], the data obtained from the process of crowdsourcing is biased towards regions with heavy human traffic. Most often, rich biodiverse regions are underrepresented limiting the performance of SDMs. In this work, we do not explicitly deal with the observation bias in presence-only SDM. However, our goal was to incorporate taxonomic information into SDM to enhance unseen species discovery.

Previous studies have evaluated species SDMs using expert range maps, which are only available for a limited number of species. Our proposed evaluation metric allows for the evaluation of SDMs using crowdsourced data, which provides a more comprehensive representation of numerous species. However, we note that none of these methods are completely free of errors. Yet, with our proposed evaluation metric, innovative methods could be developed for semi-automatic evaluation of SDMs in the future, to strike a balance between accuracy and efficiency.